

Cold Seeded Epitaxy and Flexomagnetism in GdAuGe Membranes Exfoliated From Graphene/Ge(111)

Zachary LaDuca,[†] Tamalika Samanta,[†] Nicholas Hagopian,[†] Taehwan Jung,[†]
Katherine Su,[†] Konrad Genser,[‡] Karin M. Rabe,[‡] Paul M. Voyles,[†] Michael S.
Arnold,[†] and Jason K. Kawasaki^{*,†}

*[†]Materials Science and Engineering, University of Wisconsin-Madison, Madison, WI
53706, United States of America*

[‡]Physics and Astronomy, Rutgers University, NJ 08854, United States of America

E-mail: jkawasaki@wisc.edu

Abstract

Remote and van der Waals epitaxy are promising approaches for synthesizing single crystalline membranes for flexible electronics and discovery of new properties via extreme strain; however, a fundamental challenge is that most materials do not wet the graphene surface. We develop a cold seed approach for synthesizing smooth intermetallic films on graphene that can be exfoliated to form few nanometer thick single crystalline membranes. Our seeded GdAuGe films have narrow x-ray rocking curve widths of 9-24 arc seconds, which is two orders of magnitude lower than their counterparts grown by typical high temperature methods, and have atomically sharp interfaces observed by transmission electron microscopy. Upon exfoliation and rippling, strain gradients in GdAuGe membranes induce an antiferromagnetic to ferri/ferromagnetic

transition. Our smooth, ultrathin membranes provide a clean platform for discovering new flexomagnetic effects in quantum materials.

keywords: graphene, epitaxy, membrane, Heusler, strain

Remote^{1,2} and van der Waals epitaxy^{3–6} on graphene-covered surfaces are promising strategies for synthesizing single crystalline membranes. Here, the weak van der Waals interactions between the film and graphene enable etch-free membrane exfoliation. These membranes enable applications for flexible electronics¹ and discovery of new properties induced by extreme strain.^{7–10} For example, flexomagnetism is magnetic ordering induced by strain gradients.¹¹ While there has been some success in producing strain gradients in epitaxial thin films via partial relaxation,^{12,13} greater opportunities for control exist for bending of ultrathin single crystalline membranes.¹⁴ This includes experimental demonstration of an antiferromagnetic to ferromagnetic transition in rippled GdPtSb membranes,⁹ predicted cycloidal spin textures induced by bending in CrI₃,¹⁵ and predicted bending-induced skyrmions via control of Dzyaloshinskii-Moriya Interaction (DMI) in CrBr₂ and MnSe₂,¹⁶ since strain gradients and bending break inversion symmetry.

There are two significant challenges for epitaxy on graphene. First, since graphene has very low surface energy, most materials do not wet the graphene surface and instead grow with a disconnected island morphology. This includes GaN islands on graphene/SiC,¹⁷ oxide islands on graphene/SrTiO₃,¹⁸ III-V islands^{19–21} or nanowires²² on graphene, and metal islands on graphene.^{23,24} The wetting challenge limits the ability to access the largest strains that are only possible in the ultrathin limit: whereas 8% strain has been reported for few unit cell thick (La,Ca)MnO₃ (LCMO) membranes, LCMO with thickness greater than 20 nm could only undergo 2% strain before cracking.⁷ Second, the sticking coefficients on graphene can be highly temperature and element dependent, which poses challenges for controlling the stoichiometry of alloys and compounds that are not adsorption-controlled.²⁴

Here we demonstrate a cold seeded epitaxy approach to solve the dewetting and sticking coefficient challenges. Using molecular beam epitaxy (MBE) of GdAuGe on graphene/Ge

and graphene/SiC, we demonstrate few nanometer thick films on graphene with a smooth step and terrace morphology and a 9-24 arc sec x-ray rocking curve width that is two orders of magnitude sharper than their counterparts grown at high temperature. The cold seed suppresses surface diffusion during nucleation, while subsequent annealing and continued growth at elevated temperatures recrystallizes the seed. Similar improvements in morphology have been observed for epitaxy of van der Waals materials, including Bi_2Se_3 on Si (111)²⁵ and Al_2O_3 (0001).²⁶ The cold seed also provides a template with a well defined stoichiometry, since sticking coefficients on graphene at room temperature are much closer to unity. The GdAuGe films can be exfoliated to produce continuous membranes with minimal tears that are supported on a polymer handle. We demonstrate that strain gradients in rippled GdAuGe membranes induce an antiferromagnetic to ferromagnetic transition, similar to that observed for GdPtSb membranes.⁹ We anticipate that this strategy is generally applicable to epitaxy of other thin film systems on graphene.

Figure 1 illustrates the key steps in our seeded growth approach. We start from graphene that is grown by chemical vapor deposition on Ge (111), following Ref.²⁷ After annealing the graphene in ultrahigh vacuum ($< 2 \times 10^{-10}$ Torr) at 600° C for one hour, the reflection high energy electron diffraction (RHEED) pattern along the Ge [1 $\bar{1}$ 0] azimuth exhibits a sharp ring of spots (Fig. 1a), indicating a nearly atomically smooth and clean surface. Previous low energy electron diffraction studies show that epitaxial graphene on Ge (111) has two domain orientations that are rotated 30 degrees from one another: a primary domain with graphene [1 $\bar{1}$ 00] \parallel Ge [1 $\bar{1}$ 0] and a secondary domain with graphene [1 $\bar{2}$ 10] \parallel Ge [1 $\bar{1}$ 0].²⁸

To suppress the dewetting and island formation that are typical for high temperature growth of metals on graphene surfaces,²⁴ we initiate growth of a 5 nm thick GdAuGe seed at room temperature (30°C). Here, equiatomic fluxes of Gd, Au, and Ge were supplied by thermal effusion cells at rates of 1.2×10^{13} atoms/cm²s, respectively, as measured by quartz crystal microbalance and calibrated by Rutherford backscattering spectrometry (RBS) on test samples. The corresponding RHEED pattern indicates an epitaxial seed with a semi-

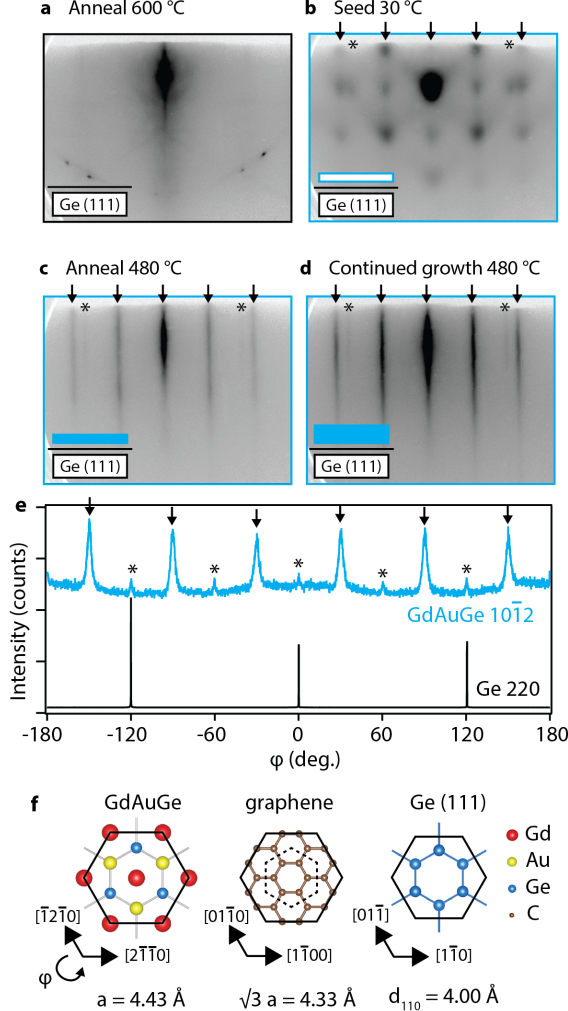


Figure 1: Cold seeded epitaxy of GdAuGe on graphene. (a) RHEED pattern of graphene on Ge (111), after annealing at 600°C to remove surface adsorbates. All RHEED patterns are recorded along a Ge $\langle 110 \rangle$ zone axis at a beam energy of 15 kV. (b) 5 nm thick seed of GdAuGe grown at 30°C. (c) Seed after recrystallizing by annealing at 480°C. (d) Continued growth of GdAuGe to a total thickness of 18 nm. Arrows mark the primary GdAuGe and graphene domain reflections. Stars mark the 30 degree rotated orientation. (e) X-ray diffraction azimuthal ϕ scan showing the in-plane epitaxial alignment. (f) Crystal structures of GdAuGe, graphene, and Ge showing the primary epitaxial alignment. For graphene, the primitive unit cell is marked by dotted lines and a $(\sqrt{3} \times \sqrt{3})R30^\circ$ supercell is marked by solid lines.

rough surface: the RHEED spots are connected by extended streaks with well-defined lattice spacings (Fig. 1b). Subsequent annealing of the seed layer at 480°C recrystallizes it and smooths the surface, as evidenced by the sharp and streaky RHEED pattern in Fig. 1(c).

The smooth surface of the annealed seed layer serves as a template for continued GdAuGe

growth at elevated temperatures. Fig. 1(d) shows the RHEED pattern of a GdAuGe film regrown at 480° C to a total thickness of 16 nm GdAuGe. The bright, sharp, and extended streaks indicate a flat epitaxial film. The final GdAuGe surface exhibits two sets of streaks: a primary set with spacing ΔQ (arrows), and a secondary set with spacing $\sqrt{3} \cdot \Delta Q$ (asterisks), indicative of two GdAuGe domains that are rotated 30 degrees from one another. An azimuthal ϕ scan by x-ray diffraction confirms two GdAuGe orientations rotated around the c axis by 30 degrees (Fig. 1(e)).

An interesting question is whether GdAuGe films on graphene/Ge are epitaxial to the graphene or to the Ge substrate, e.g., via “remote” substrate interactions that permeate through graphene.¹ Here we find a direct correspondence between two graphene orientations rotated by 30 degrees, and two GdAuGe orientations rotated by 30 degrees. In contrast, growth of GdAuGe directly on Ge (111) produces only a single domain orientation. Thus the presence of two GdAuGe domain orientations on graphene/Ge(111) suggests the primary epitaxial relationship is between GdAuGe and graphene, which are in direct contact, rather than GdAuGe and the Ge via a remote interaction through the graphene. The lattice mismatch of 2.3% between GdAuGe and a $(\sqrt{3} \times \sqrt{3})R30^\circ$ supercell of graphene is smaller than the 9.7% mismatch between GdAuGe and Ge (111) (Fig. 1(f)), which also suggests a preferred epitaxial relationship to graphene.

As an additional test, we grew GdAuGe on graphene/Ge(110), where the Ge (110) surface has rectangular symmetry compared to the hexagonal symmetry of GdAuGe. We find that GdAuGe again grows (0001)-oriented, with the same in-plane orientation with respect to graphene: GdAuGe $[2\bar{1}\bar{1}0] \parallel$ graphene $[1\bar{1}00]$ (Supplemental Figure 1).

Figure 2 compares the structure and morphology of a 16 nm GdAuGe film grown with a cold seeded growth approach on graphene/Ge(111) to that of an 18 nm film grown directly on graphene/Ge(111) at 540°C. For the seeded sample, the $2\theta - \omega$ x-ray diffraction scan displays bright GdAuGe $000l$ reflections, including the higher order 0006 and 0008 Bragg reflections. The sharp Kiessig fringes around the GdAuGe 0004 reflection (insert) indicate

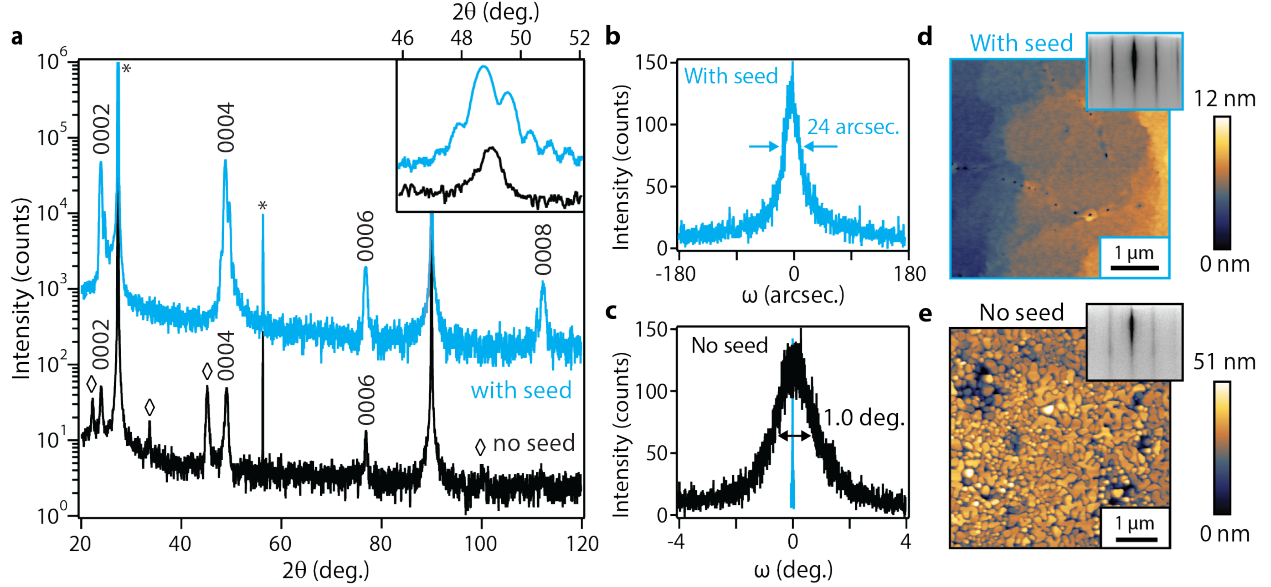


Figure 2: **Comparison of low temperature seeded growth versus direct high temperature growth of GdAuGe on graphene/Ge (111).** (a) X-ray diffraction scan (Cu $K\alpha$) of a film grown using the low temperature seed approach (blue) versus a film grown directly at high temperature (black). Insert shows the 0004 reflection. (b,c) Rocking curves of 0004 reflection for the seeded and unseeded samples. (d,e) Atomic force microscopy showing a step and terrace morphology for the seeded sample and an island morphology for the no seed sample. Insets show the RHEED patterns at the end of GdAuGe growth.

a smooth surface and interface morphology (Fig. 2(a), blue trace). These x-ray fringes are consistent with the narrow x-ray rocking curve width of 24 arc seconds that indicates a low mosaicity (Fig. 2(b)). This rocking curve width is significantly narrower than the 245 arc sec reported for GaAs on graphene/SiO₂,¹⁹ 300 arc sec for GaN on graphene/GaN,²⁹ 115 arc sec for SrTiO₃ on graphene/SrTiO₃,³⁰ 180 arc sec for VO₂ on graphene,³¹ 770 arc sec for ZnO on graphene,³² and 1.2 degrees (4320 arc sec) for BaTiO₃ on graphene/Ge (110).³³ We observe a flat atomic step and terrace morphology by atomic force microscopy (AFM, Fig. 2(d)). In the AFM scan we also observe an arc of circular openings with depth of a few nanometers into the sample. We attribute these depressions to defects induced by a graphene grain boundary or wrinkle.

In contrast, the sample without seed layer displays weaker 000l reflections, indicative of poorer crystallinity, no Kiessig fringes, and XRD reflections from secondary phases (diamond

symbols). We attribute the secondary phases to the fact that the sticking coefficients of metals on graphene deviate significantly from unity at elevated temperatures, as observed previously for other metals on graphene,²⁴ and confirmed for GdAuGe on graphene by RBS (Supplemental Fig. 2). This nonstoichiometry at high growth temperature could in principle be compensated by adjusting the incident flux ratios. However, since the dewetted film surface contains both GdAuGe islands and exposed graphene, whose area fraction is changing over time, true compensation requires continuously changing the incident flux ratios.²⁴ The low temperature seed layer solves this challenge by establishing a continuous, GdAuGe-covered surface with no dewetting within the first few atomic layers. AFM of the non seeded sample displays a disconnected island morphology (Fig. 2e), consistent with large rocking curve width of 1 degree that indicates large mosaicity (Fig. 2c).

Cross-sectional high angular annular dark field (HAADF) STEM imaging of the seeded sample reveals a well ordered GdAuGe /graphene/Ge interface (Figure 3). The GdAuGe /graphene/Ge interface appears atomically sharp, terminated with an Au/Ge plane above the graphene interface. Due to Z-contrast image intensity, heavier elements such as Gd and Au are bright and easily visible whereas lighter carbon in the graphene layer exhibits a relatively weak signal. Just below the graphene, the top layer of the Ge substrate displays brighter contrast than the bulk Ge substrate, indicating possible Gd intercalation. Gd intercalation under graphene has been reported previously, although at slightly higher temperatures of 800°C,³⁴ compared to the 30° C deposition and 480°C anneal and regrowth we employ here. Finally, we observe that the film is a continuous single crystal between the annealed seed layer and continued growth layer, with no obvious defects induced by the temperature cycling. Our combined diffraction (XRD and RHEED), surface topography (AFM), and electron microscopy support the enhanced structural quality and smoothness for films grown by our low temperature seed approach compared to direct growth at elevated temperature.

Our low temperature seed layer approach appears generalizable to other graphene-covered substrates. As shown in Supplementary Fig. 3, seeded GdAuGe growth on graphene/SiC

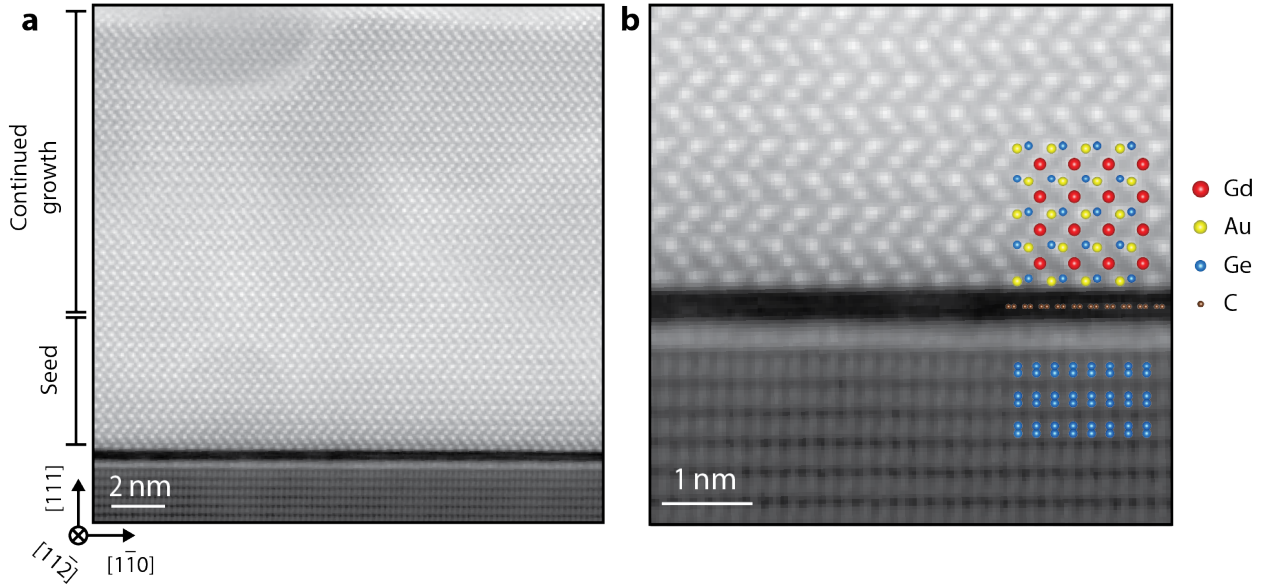


Figure 3: High-angle annular dark-field scanning transmission electron microscopy (HAADF-STEM) of GdAuGe/graphene/Ge(111). (a) Wide field of view showing a highly ordered film with no boundary between seed and continued growth. (b) Zoom in showing a sharp GdAuGe/graphene/Ge interface.

(0001) produces films with narrower rocking curve width ($\Delta\omega = 9$ arc sec), smoother AFM morphology, and sharper Kiessig fringes compared to films grown directly at high temperature. Additionally, the seeded samples show the expected metallic transport, compared to the hopping transport observed for high temperature growth due to the disconnected island morphology (Supplementary Fig. 4).

Our smooth GdAuGe films grown using the seed approach provide an excellent starting point for membrane exfoliation and manipulation of magnetic properties via extreme strain. To produce membranes with large strain gradients, we adhere a polyurethane handle under tensile strain to the GdAuGe film and exfoliate by cooling the sample in liquid nitrogen. Upon exfoliation, the polyurethane contracts to induce ripples in the GdAuGe membrane. For GdAuGe films grown with a seed layer, this exfoliation produces continuous membranes with well ordered ripples over length scales of several hundred of microns (Fig. 4(a) insert and Supplemental Fig. 5). In contrast, exfoliation of samples grown directly at high temperature on graphene/Ge show a rough and disconnected morphology with no ripples, suggesting that

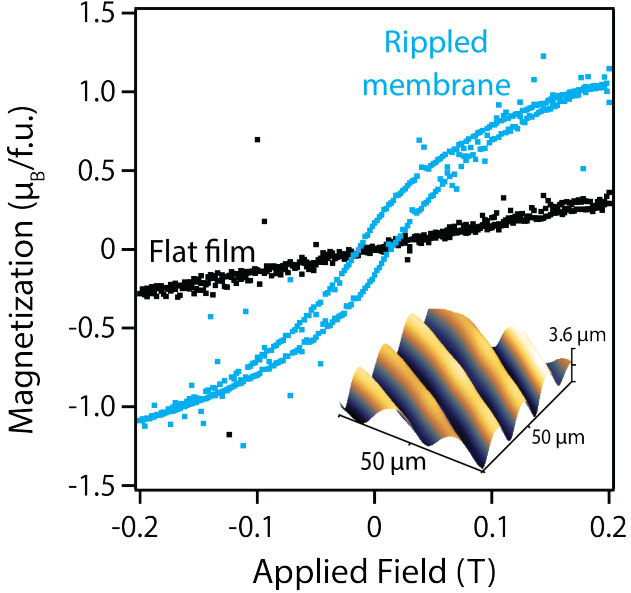


Figure 4: SQUID magnetometry at 2K demonstrating strain gradient induced ferri/ferromagnetism in a rippled GdAuGe membrane (blue curve), compared to the antiferromagnetic flat film (black curve). The field orientation was in plane. Insert shows AFM topography of the rippled membrane.

the polymer contraction does not produce a well controlled strain pattern in the unseeded samples.

Fig. 4 compares SQUID magnetometry of a rippled GdAuGe membrane grown using the seed layer, compared with a relaxed GdAuGe film. At the measurement temperature of 2 K, the film shows a weak linear dependence of magnetization on applied field, consistent with the antiferromagnetism observed in bulk crystals.^{35–37} In contrast, the rippled sample displays a clear hysteresis loop indicative of ferro or ferrimagnetic ordering. The behavior is similar to GdPtSb membranes for which we also observe bending-induced ferri/ferromagnetism,⁹ but with a factor of 5 smaller magnetic saturation than GdPtSb at similar bend radius.

An important distinction is whether the magnetic ordering is induced by homogeneous strain (piezomagnetism and magnetotstriction) or by strain gradients (flexomagnetism). For a smoothly curved membrane with no plastic deformation, the strain along the curved path s is approximately $\varepsilon_s \approx (R+t)/R - 1$, where t is the height or depth along the thickness axis and R is the radius of curvature.⁹ Based on the measured thickness of 20 nm, period of 12

μm , and peak to peak height of $2.6 \mu\text{m}$, we estimate a maximum strain of $\varepsilon_s \approx \pm 0.36\%$ and maximum strain gradient of $\partial\varepsilon_s/\partial z \approx \pm 36\%/\mu\text{m}$ at the peaks and valleys. Compared with our density functional theory calculations of antiferromagnetic vs ferromagnetic ordering (Supplemental Figure 6), we find that the peak strain in our rippled membrane is an order of magnitude smaller than the calculated homogeneous strain to induce ferromagnetic ordering. This suggests that coupling to strain gradients is more likely responsible for the observed ferro/ferrimagnetic ordering than coupling to homogeneous strain, similar to GdPtSb.⁹ We note, however, that the antiferromagnetic ordering of GdAuGe has not yet been solved,³⁵ and in our calculation we assume *A*-type ordering with moments pointed along *c*. The particular choice of AFM structure will change the expected strain induced crossover between AFM and FM ordering. Further experiments and theory are required to solve the magnetic structure of GdAuGe and understand its response to strain and strain gradients.

In conclusion, we demonstrated a cold seeded epitaxy approach for growing few nanometer thick, smooth GdAuGe films on graphene-covered Ge and SiC substrates. Seeded films display sharper Bragg reflections, lower mosaicity, and a smoother atomic step and terrace morphology than their counterparts grown directly at high temperature. These films are epitaxial to graphene rather than the underlying Ge or SiC substrate. The interfaces with graphene are atomically sharp. Using a rippled membrane exfoliate from graphene, we demonstrated an antiferromagnetic to ferri/ferromagnetic transition induced by strain gradients. This flexomagnetic response is similar to GdPtSb. Our cold seed strategy provides a path for access to extreme strains in membranes in the ultrathin limit.

Supporting Information

Supporting Information contains experimental and theoretical methods, tests of epitaxial relationship of GdAuGe to graphene versus germanium, electrical transport of seeded versus unseeded films, and morphology of exfoliated membranes.

Data Availability

All raw data that appears in this manuscript are posted on Zenodo, reference number 12785490 (<https://zenodo.org/records/12785490>).

Acknowledgments

We thank Chengye Dong and Joshua Robinson at The Pennsylvania State University Two-Dimensional Crystal Consortium – Materials Innovation Platform (2DCC-MIP) for graphene on SiC samples. 2DCC-MIP is supported by NSF cooperative agreement DMR-2039351. We thank Greg Haugstad at the University of Minnesota Characterization Facility for RBS measurements.

This project was primarily supported by the the Department of Energy Office of Science (DE-SC00203958, Heusler synthesis by Z.L., T.S., T.J., and J.K.K.). Magnetic measurements (Z.L., T.S., and J.K.K.) and electron microscopy (N.H. and P.M.V.) were supported by NSF through the University of Wisconsin Materials Research Science and Engineering Center (DMR-2309000). We acknowledge user facilities also supported by the Wisconsin MRSEC. Transport and preliminary synthesis (Z.L. and J.K.K.) were supported by the Air Force Office of Scientific Research (FA9550-21-0127). Graphene on germanium synthesis and characterization (K.S. and M.S.A.) are supported by the U.S. Department of Energy, Office of Science, Basic Energy Sciences, (DE-SC0016007) and the NSF Graduate Research Fellowship Program (DGE-1747503). DFT calculations (K.T.G. and K.M.R.) were supported by the Office of Naval Research (ONR N00014-21-1-2107) and Wisconsin MRSEC.

References

- (1) Kim, Y.; Cruz, S. S.; Lee, K.; Alawode, B. O.; Choi, C.; Song, Y.; Johnson, J. M.; Heidelberger, C.; Kong, W.; Choi, S.; others Remote epitaxy through graphene enables

two-dimensional material-based layer transfer. *Nature* **2017**, *544*, 340–343.

(2) Kong, W.; Li, H.; Qiao, K.; Kim, Y.; Lee, K.; Nie, Y.; Lee, D.; Osadchy, T.; Molnar, R. J.; Gaskill, D. K.; others Polarity governs atomic interaction through two-dimensional materials. *Nature materials* **2018**, *17*, 999–1004.

(3) Koma, A. Van der Waals epitaxy—a new epitaxial growth method for a highly lattice-mismatched system. *Thin Solid Films* **1992**, *216*, 72–76.

(4) Shi, Y.; Zhou, W.; Lu, A.-Y.; Fang, W.; Lee, Y.-H.; Hsu, A. L.; Kim, S. M.; Kim, K. K.; Yang, H. Y.; Li, L.-J.; others van der Waals epitaxy of MoS₂ layers using graphene as growth templates. *Nano letters* **2012**, *12*, 2784–2791.

(5) Kim, J.; Bayram, C.; Park, H.; Cheng, C.-W.; Dimitrakopoulos, C.; Ott, J. A.; Reuter, K. B.; Bedell, S. W.; Sadana, D. K. Principle of direct van der Waals epitaxy of single-crystalline films on epitaxial graphene. *Nature communications* **2014**, *5*, 4836.

(6) Du, D.; Jung, T.; Manzo, S.; LaDuca, Z.; Zheng, X.; Su, K.; Saraswat, V.; McChesney, J.; Arnold, M. S.; Kawasaki, J. K. Controlling the balance between remote, pinhole, and van der Waals epitaxy of Heusler films on graphene/sapphire. *Nano Letters* **2022**, *22*, 8647–8653.

(7) Hong, S. S.; Gu, M.; Verma, M.; Harbola, V.; Wang, B. Y.; Lu, D.; Vailionis, A.; Hikita, Y.; Pentcheva, R.; Rondinelli, J. M.; others Extreme tensile strain states in La_{0.7}Ca_{0.3}MnO₃ membranes. *Science* **2020**, *368*, 71–76.

(8) Harbola, V.; Crossley, S.; Hong, S. S.; Lu, D.; Birkholzer, Y. A.; Hikita, Y.; Hwang, H. Y. Strain gradient elasticity in SrTiO₃ membranes: bending versus stretching. *Nano letters* **2021**, *21*, 2470–2475.

(9) Du, D.; Manzo, S.; Zhang, C.; Saraswat, V.; Genser, K. T.; Rabe, K. M.; Voyles, P. M.; Arnold, M. S.; Kawasaki, J. K. Epitaxy, exfoliation, and strain-induced magnetism in rippled Heusler membranes. *Nature communications* **2021**, *12*, 1–7.

(10) Dong, G.; Li, S.; Yao, M.; Zhou, Z.; Zhang, Y.-Q.; Han, X.; Luo, Z.; Yao, J.; Peng, B.; Hu, Z.; others Super-elastic ferroelectric single-crystal membrane with continuous electric dipole rotation. *Science* **2019**, *366*, 475–479.

(11) Lukashev, P.; Sabirianov, R. F. Flexomagnetic effect in frustrated triangular magnetic structures. *Physical Review B* **2010**, *82*, 094417.

(12) Zhang, Y.; Liu, J.; Dong, Y.; Wu, S.; Zhang, J.; Wang, J.; Lu, J.; Rückriegel, A.; Wang, H.; Duine, R.; others Strain-driven Dzyaloshinskii-Moriya interaction for room-temperature magnetic skyrmions. *Physical Review Letters* **2021**, *127*, 117204.

(13) Makushko, P.; Kosub, T.; Pylypovskiy, O. V.; Hedrich, N.; Li, J.; Pashkin, A.; Avdoshenko, S.; Hübner, R.; Ganss, F.; Wolf, D.; others Flexomagnetism and vertically graded Néel temperature of antiferromagnetic Cr₂O₃ thin films. *Nature Communications* **2022**, *13*, 6745.

(14) Du, D.; Hu, J.; Kawasaki, J. K. Strain and strain gradient engineering in membranes of quantum materials. *Applied Physics Letters* **2023**, *122*, 170501.

(15) Edström, A.; Amoroso, D.; Picozzi, S.; Barone, P.; Stengel, M. Curved magnetism in CrI₃. *Physical review letters* **2022**, *128*, 177202.

(16) Ga, Y.; Cui, Q.; Liang, J.; Yu, D.; Zhu, Y.; Wang, L.; Yang, H. Dzyaloshinskii-Moriya interaction and magnetic skyrmions induced by curvature. *Physical Review B* **2022**, *106*, 054426.

(17) Qiao, K.; Liu, Y.; Kim, C.; Molnar, R. J.; Osadchy, T.; Li, W.; Sun, X.; Li, H.;

Myers-Ward, R. L.; Lee, D.; others Graphene buffer layer on SiC as a release layer for high-quality freestanding semiconductor membranes. *Nano letters* **2021**, *21*, 4013–4020.

(18) Chang, C. S.; Kim, K. S.; Park, B.-I.; Choi, J.; Kim, H.; Jeong, J.; Barone, M.; Parker, N.; Lee, S.; Zhang, X.; others Remote epitaxial interaction through graphene. *Science Advances* **2023**, *9*, eadj5379.

(19) Alaskar, Y.; Arafin, S.; Wickramaratne, D.; Zurbuchen, M. A.; He, L.; McKay, J.; Lin, Q.; Goorsky, M. S.; Lake, R. K.; Wang, K. L. Towards van der Waals epitaxial growth of GaAs on Si using a graphene buffer layer. *Advanced Functional Materials* **2014**, *24*, 6629–6638.

(20) Zulqurnain, M.; Burton, O. J.; Al-Hada, M.; Goff, L. E.; Hofmann, S.; Hirst, L. C. Defect seeded remote epitaxy of GaAs films on graphene. *Nanotechnology* **2022**, *33*, 485603.

(21) Manzo, S.; Strohbeen, P. J.; Lim, Z. H.; Saraswat, V.; Du, D.; Xu, S.; Pokharel, N.; Mawst, L. J.; Arnold, M. S.; Kawasaki, J. K. Pinhole-seeded lateral epitaxy and exfoliation of GaSb films on graphene-terminated surfaces. *Nature communications* **2022**, *13*, 1–9.

(22) Hong, Y. J.; Lee, W. H.; Wu, Y.; Ruoff, R. S.; Fukui, T. van der Waals epitaxy of InAs nanowires vertically aligned on single-layer graphene. *Nano letters* **2012**, *12*, 1431–1436.

(23) Liu, X.; Wang, C.-Z.; Hupalo, M.; Lin, H.-Q.; Ho, K.-M.; Tringides, M. C. Metals on graphene: interactions, growth morphology, and thermal stability. *Crystals* **2013**, *3*, 79–111.

(24) LaDuca, Z.; Su, K.; Manzo, S.; Arnold, M. S.; Kawasaki, J. K. Control of ternary alloy composition during remote epitaxy on graphene. *Physical Review Materials* **2023**, *7*, 083401.

(25) Bansal, N.; Kim, Y. S.; Edrey, E.; Brahlek, M.; Horibe, Y.; Iida, K.; Tanimura, M.; Li, G.-H.; Feng, T.; Lee, H.-D.; others Epitaxial growth of topological insulator Bi₂Se₃ film on Si (111) with atomically sharp interface. *Thin Solid Films* **2011**, *520*, 224–229.

(26) Wang, Y.; Ginley, T. P.; Law, S. Growth of high-quality Bi₂Se₃ topological insulators using (Bi_{1-x}In_x)₂Se₃ buffer layers. *Journal of Vacuum Science & Technology B* **2018**, *36*.

(27) Manzo, S.; Su, K.; Arnold, M. S.; Kawasaki, J. K. Nucleation Selectivity and Lateral Coalescence of GaAs over Graphene on Ge (111). *ACS Applied Materials & Interfaces* **2023**, *15*, 59905–59911.

(28) Kiraly, B.; Jacobberger, R. M.; Mannix, A. J.; Campbell, G. P.; Bedzyk, M. J.; Arnold, M. S.; Hersam, M. C.; Guisinger, N. P. Electronic and mechanical properties of graphene–germanium interfaces grown by chemical vapor deposition. *Nano letters* **2015**, *15*, 7414–7420.

(29) Badokas, K.; Kadys, A.; Mickevičius, J.; Ignatjev, I.; Skapas, M.; Stanionytė, S.; Radiunas, E.; Juška, G.; Malinauskas, T. Remote epitaxy of GaN via graphene on GaN/sapphire templates. *Journal of Physics D: Applied Physics* **2021**, *54*, 205103.

(30) Yoon, H.; Truttmann, T. K.; Liu, F.; Matthews, B. E.; Choo, S.; Su, Q.; Saraswat, V.; Manzo, S.; Arnold, M. S.; Bowden, M. E.; others Freestanding epitaxial SrTiO₃ nanomembranes via remote epitaxy using hybrid molecular beam epitaxy. *Science Advances* **2022**, *8*, eadd5328.

(31) Guo, Y.; Sun, X.; Jiang, J.; Wang, B.; Chen, X.; Yin, X.; Qi, W.; Gao, L.; Zhang, L.; Lu, Z.; others A reconfigurable remotely epitaxial VO₂ electrical heterostructure. *Nano letters* **2019**, *20*, 33–42.

(32) Wang, N.; Wang, P.; Wang, F.; He, H.; Huang, J.; Pan, X.; Zhu, G.; Wang, J.; Ye, Z.

Improved epitaxy of ZnO films by regulating the layers of graphene. *Applied Surface Science* **2022**, *585*, 152709.

- (33) Dai, L.; Zhao, J.; Li, J.; Chen, B.; Zhai, S.; Xue, Z.; Di, Z.; Feng, B.; Sun, Y.; Luo, Y.; others Highly heterogeneous epitaxy of flexoelectric BaTiO₃- δ membrane on Ge. *Nature Communications* **2022**, *13*, 1–10.
- (34) Link, S.; Forti, S.; Stöhr, A.; Küster, K.; Rösner, M.; Hirschmeier, D.; Chen, C.; Avila, J.; Asensio, M.; Zakharov, A.; others Introducing strong correlation effects into graphene by gadolinium intercalation. *Physical Review B* **2019**, *100*, 121407.
- (35) Ram, D.; Singh, J.; Hooda, M.; Singh, K.; Kanchana, V.; Kaczorowski, D.; Hosain, Z. Multiple magnetic transitions, metamagnetism, and large magnetoresistance in GdAuGe single crystals. *Physical Review B* **2023**, *108*, 235107.
- (36) Kurumaji, T.; Gen, M.; Kitou, S.; Arima, T.-h. Metamagnetism and anomalous magnetotransport properties in rare-earth-based polar semimetals R AuGe (R = Dy, Ho, and Gd). *arXiv* **2024**, 2405.00628, doi:10.48550/arXiv.2405.00628, accessed 2024-08-07.
- (37) Gibson, B.; Schnelle, W.; Pöttgen, R.; Bartkowski, K.; Kremer, R. Susceptibility, specific heat, and transport properties of CeAuGe and GdAuGe. *Czechoslovak Journal of Physics* **1996**, *46*, 2573–2574.

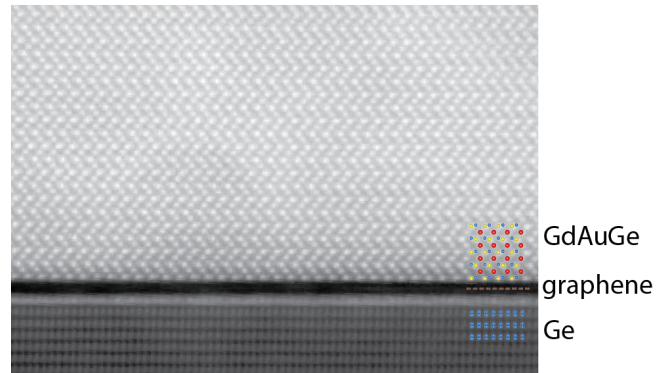


Figure 5: TOC figure